Structural Transformation of Surface-Confined Porphyrin Networks by Addition of Co Atoms

Special Collection

Brian D. Baker Cortés[+],[a] Mihaela Enache[+],[a] Kathrin Küster,[a, b] Florian Studener,[a] Tien-Lin Lee,[c] Nicolas Marets,[d] Véronique Bulach,*[d] Mir Wais Hosseini,*[d] and Meike Stöhr*[a]

Abstract: The self-assembly of a nickel-porphyrin derivative (Ni-DPPyP) containing two pyridyl coordinating sites and two pentyl chains at *trans meso* positions was studied with scanning tunneling microscopy (STM), X-ray photoelectron spectroscopy (XPS) and low energy electron diffraction (LEED) on Au(111). Deposition of Ni-DPPyP onto Au(111) gave rise to a close-packed network for coverages smaller or equal to one monolayer as revealed by STM and LEED. The molecular arrangement of this two-dimensional network is stabilized via hydrogen bonds formed between the pyridyl's nitrogen and hydrogen atoms from the pyrrole groups of neighboring molecules. Subsequent deposition of cobalt atoms onto the close-packed network and post-deposition annealing at 423 K led to the formation of a Co-coordinated hexagonal porous network. As confirmed by XPS measurements, the porous network is stabilized by metal-ligand interactions between one cobalt atom and three pyridyl ligands, each pyridyl ligand coming from a different Ni-DPPyP molecule.

Introduction

The well-established protocols of supramolecular chemistry have opened a pathway for the bottom-up fabrication of nanostructures on surfaces.[1–3] In particular, self-assembled two-dimensional (2D) networks on noble metal surfaces formed by a countless variety of organic building blocks interconnected by metal-ligand interactions – better known as metal-organic coordination networks (MOCNs) – have been a subject of study due to their intriguing properties and prospective usage in technological applications.[4–8] To this end, porphyrins are known to be highly versatile building blocks for the construction of metal-directed 2D assemblies since their macrocycle can be decorated with different substituents that can coordinate to metal atoms in a variety of distinctive coordination geometries.[7,9–13] However, the formation of porphyrin-based MOCNs exhibiting a porous structure, i.e., with cavities in the order of a few nm, have been rarely reported.[14–16] Furthermore, the (structural) properties of porous MOCNs allows them to be used as hosts for guest molecules and for the fabrication of quantum corrals.[11,17] Moreover, porous MOCNs can possess intriguing magnetic properties by the inclusion of magnetic centers within their structure, for example, through metallation of the porphyrin core.[6,14,15,18–21]

The characterization of MOCNs on noble metal surfaces has been conducted, in most of the cases, by means of scanning tunneling microscopy (STM) owing to its supreme imaging capabilities under ultra-high vacuum (UHV) conditions. Surprisingly, the use of photoemission spectroscopies, that is X-ray photoelectron spectroscopy (XPS) – which does not only provide information about the elements present on the surface but also about their chemical state – has been rarely used to characterize MOCNs, i.e., to investigate the fingerprint of the metal-ligand interactions.[22] Furthermore, XPS measurements can be used to determine if the metal-ligand interaction only affects the chemical state of the coordinating atom or if it

[a] *B. D. Baker Cortés,[+] Dr. M. Enache,[+] Dr. K. Küster, F. Studener, Prof. Dr. M. Stöhr*
Zernike Institute for Advanced Materials
University of Groningen
Nijenborgh 4, 9747 AG, Groningen (The Netherlands)
E-mail: m.a.stohr@rug.nl

[b] *Dr. K. Küster*
Present address: Max-Planck-Institut für Festkörperforschung
Heisenbergstraße 1, 70569 Stuttgart (Germany)

[c] *Dr. T.-L. Lee*
Diamond Light Source
Harwell Science and Innovation Campus
Didcot, OX11 0DE (UK)

[d] *N. Marets, Prof. Dr. V. Bulach, Prof. Dr. M. W. Hosseini*
Laboratoire de Tectonique Moléculaire
UMR Unistra-CNRS 7140
Université de Strasbourg
4 rue BlaisePascal, 67070 Strasbourg (France)
E-mail: bulach@unistra.fr
hosseini@unistra.fr

[+] *These authors contributed equally to this work.*

Supporting information for this article is available on the WWW under https://doi.org/10.1002/chem.202101217

Special Collection *This article belongs to a Joint Special Collection dedicated to François Diederich.*

influences additional atoms such as the entire coordinating group or molecule.

Herein, we report the self-assembly behavior of nickel(II) 5,15-dipentyl-10,20-(4-yl-pyridine)porphyrin (Ni-DPPyP)[16] before and after coordination with Co-atoms on Au(111) by means of STM, XPS and low-energy electron diffraction (LEED). As shown in Scheme 1, Ni-DPPyP is a Ni-substituted porphyrin derivative functionalized at *trans meso* positions by two pyridyl and two pentyl chains. As revealed by STM and LEED measurements, the deposition of Ni-DPPyP on Au(111) gave rise to the formation of long-range ordered close-packed assemblies stabilized by H-bonds. C 1s and N 1s core level X-ray photoelectron spectra were acquired to give insight to the chemical composition of the Ni-DPPyP on Au(111) prior to Co-deposition. The binding energy (BE) value for the pyridylic N 1s core level was in agreement with the previously reported peak positions for N-atoms involved in H-bonding.[22–24] The deposition of Co-atoms at room-temperature (RT) and post-deposition annealing at 423 K prompted a structural transformation, i.e., the close-packed assembly rearranged into a hexagonal porous network as observed with STM and LEED. This hexagonal network contains pores that are formed by six molecules and each pore is interconnected by three-fold Co-coordination nodes. The transformation from a H-bonding to a metal-ligand interaction by deposition of the Co-atoms was corroborated by the chemical shifts of the N 1s and C 1s XPS signals toward higher BE, which was most prominent for the N in the pyridyl group binding to the Co-atoms. From a structural point of view, our results are in agreement with the 2D assemblies reported in our previous study of the free-base version of Ni-DPPyP on Ag(111), where a structurally equivalent porous MOCN was formed at RT after the deposition of Co-atoms and upon annealing at 450 K, the Co-atoms that were coordinating the network diffused along the Ag(111) surface and metalated the porphyrin core. This lead to a structural transformation of the porous MOCN into a non-metal coordinated close-packed network.[16] However, in our present study we focused on fabricating a similar porous network on Au(111) with higher thermal stability by incorporating a Ni-atom in the porphyrin core in order to avoid the metalation of the porphyrin core with Co-atoms upon annealing.

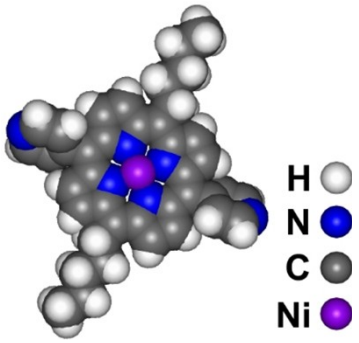

Scheme 1. Schematic molecular structure of nickel(II) 5,15-dipentyl-10,20-(4-yl-pyridine)porphyrin (Ni-DPPyP).

Results and Discussion

Upon deposition of a submonolayer of Ni-DPPyP on Au(111) at RT, a close-packed assembly was formed as shown in the overview STM image of Figure 1. Two different rotational domains (I and II) of the network can be observed on each side of the step edge of the Au substrate. In addition, the intact herringbone reconstruction of the Au substrate beneath the organic layer implies a weak molecule-substrate interaction (Supporting Information Figure S1). The dotted white square in Figure 1a corresponds to the area from which the bias dependent STM image of Ni-DPPyP (Figure 1b) was acquired. The pyridyl and pentyl endgroups are imaged as bright round and long protrusions (at all given biases), respectively. One Ni-DPPyP molecule is added to guide the eye. The out-of-plane rotation of the pyridyl endgroups with respect to the porphyrin macrocycle confers them with an enhanced STM contrast over the remnant moieties of Ni-DPPyP.[16,27,28] The porphyrin macrocycle remained dim at both bias polarities and the Ni-atom did not contribute to the STM contrast, in line with earlier reports.[11]

The long-range order of the network was confirmed by our LEED measurements (Figure 2) and in combination with the STM data, we constructed a unit cell with dimensions $a = 14.1 \pm 0.1$ Å, $b = 14.9 \pm 0.1$ Å, and an internal angle of $\alpha = 88° \pm 2°$. The molecular density amounts to 0.48 Ni-DPPyP molecules per nm^2. The unit cell is rotated by 15° with respect to the principal Au directions. The close-packed network is incommensurate with respect to the underlying Au substrate as supported by the absence of integer matrix elements in the superstructure matrix of the simulated LEED pattern (Figure 2b). The presence of three rotationally equivalent and three mirror domains was corroborated by the LEED measurements (Figure 2a). This was supported by the simulated LEED pattern (Figure 2b), which shows the unit cell (black square) with the rotationally equivalent and mirror domains of the assembly depicted by the

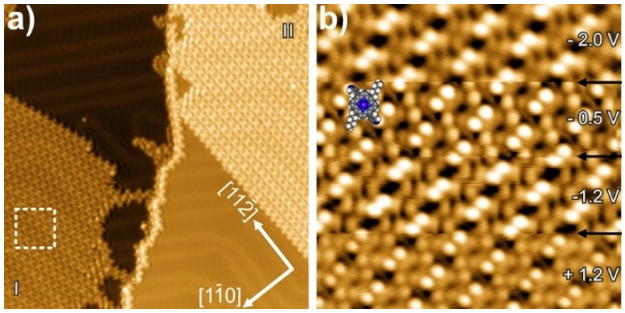

Figure 1. For submonolayer coverage of Ni-DPPyP on Au(111) a close-packed arrangement develops. (a) Overview STM image (42×42 nm^2, U = −1.2 V, I = 20 pA, 77 K) in which two rotational domains (labelled I and II) of the close-packed assembly are visible. The substrate directions are denoted by the white arrows. (b) Bias voltage-dependent close-up STM image (10×10 nm^2, I = 20 pA, 77 K) for the area indicated by the white dashed square in (a). The intramolecular features of Ni-DPPyP (pyridyl units, alkyl chains as well as the porphyrin core) can be discerned. For clarity, a molecule is superimposed on the STM image. The black arrows indicate the scan lines where the bias was changed. The corresponding bias voltages are indicated in the image.

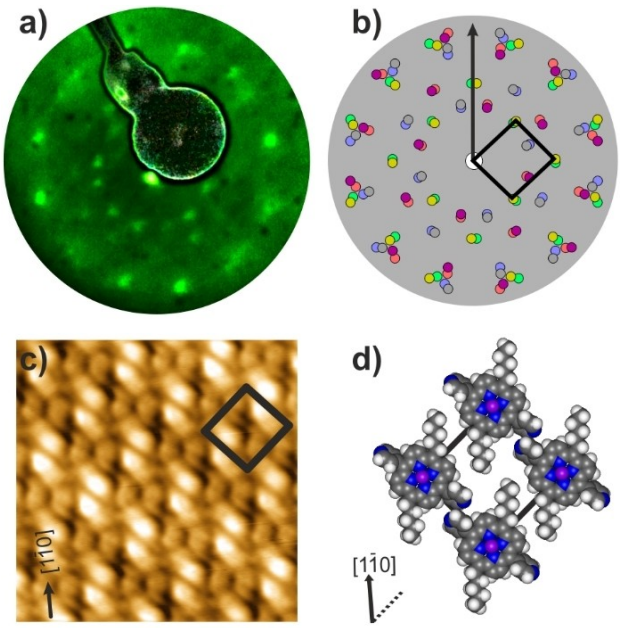

Figure 2. (a) Experimentally obtained LEED pattern for submonolayer coverage of Ni-DPPyP on Au(111) taken at a beam energy of 12.2 eV. (b) Simulated LEED pattern. The different colors mark the rotationally equivalent and mirrored domains. The black square indicates the molecular unit cell for one of the domains of the molecular adlayer. The black arrow shows the close-packed [1$\bar{1}$0] direction of the Au(111) surface. (c) High-resolution STM image (6.4×6.4 nm^2, U = −3 V, I = 20 pA, 77 K) for the close-packed arrangement where the unit cell is marked by the black rectangle. (d) Tentative model for the molecular arrangement of Ni-DPPyP on Au(111). The black arrows at the bottom left corner in (c) and (d) indicate the close-packed [1$\bar{1}$0] direction of the Au(111) surface. The dotted black line in (d) is parallel to a unit cell direction. The superstructure of the simulated LEED pattern is described by the matrix notation $\begin{pmatrix} 5.5 & 1.5 \\ 1.7 & 5.8 \end{pmatrix}$.

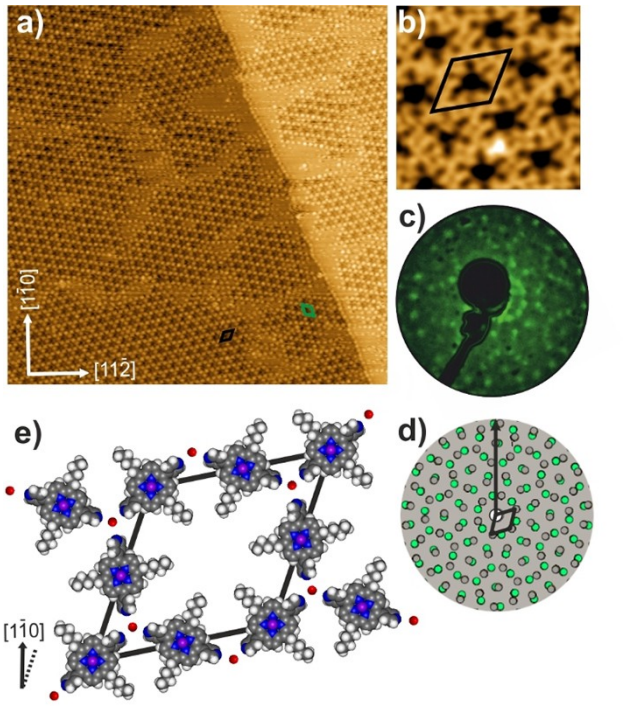

Figure 3. Cobalt-coordinated porous network of Ni-DPPyP on Au(111). (a) Overview STM image (113×113 nm^2, U = 2 V, I = 20 pA, RT). The two different domains are marked by the black and green rhombic unit cell. (b) Close-up STM image (10.8×10.8 nm^2, U = −3.5 V, I = 20 pA, RT) of the cobalt-coordinated porous network. (c) Experimentally obtained LEED pattern for the cobalt-coordinated porous network of Ni-DPPyP on Au(111) taken at a beam energy of 8.3 eV. (d) Simulated LEED pattern. The different colors mark the two domains. The black square indicates the molecular unit cell for one of the domains of the molecular adlayer. The dotted black arrow shows the close-packed [1$\bar{1}$0] direction of the Au(111) surface. (e) Tentative structural model for the cobalt-coordinated porous Ni-DPPyP network. One cobalt atom (orange circles) coordinates to three pyridyl ligands. The unit cell is indicated by the black rhombus. The black arrow indicates the close-packed [1$\bar{1}$0] direction of the Au(111) surface. The dotted black line in (e) is parallel to a unit cell direction. The superstructure of the simulated LEED pattern is described by the matrix notation $\begin{pmatrix} 9.1 & 3.3 \\ -3.3 & 12.4 \end{pmatrix}$.

spots in different colors. Furthermore, the orientation of the molecules with respect to each other can be discerned within the unit cell (black square) overlaid in Figure 2c, where the pyridyl endgroups of neighboring Ni-DPPyP molecules align parallel to each other. This arrangement is similar to the orientation observed for tetraphenyl and tetrapyridyl porphyrins on metal substrates.[29–31] As shown in the tentative structural model (Figure 2d) the 2D network is stabilized by H-bonding between the electronegative N-atom of the pyridyl endgroup and one H-atom from a neighboring pyrrole moiety.[29,31] Additionally, the pentyl chains interact with the neighboring pentyl and pyrrolic moieties via van der Waals interactions.[16]

The deposition of Co-atoms onto a submonolayer of the close-packed network followed by post-deposition annealing at 423 K led to the formation of a porous 2D network (Figure 3). The presence of two rotational domains, which are mirror domains with respect to each other when mirrored at a principal Au direction, is highlighted by the green and black rhombuses (Figure 3a). In contrast to the close-packed network, the herringbone reconstruction of the Au substrate was no longer visible through the molecular layer. It could be that this has to be ascribed to the imaging parameters and tip condition but we do not rule out the possibility that the herringbone reconstruction might have been partially lifted by the formation of the Co-coordinated porous network, i.e., the interaction of the Co-atoms with the Au surface might be stronger than the molecule-substrate interactions in the close-packed network. The close-up STM image (Figure 3b) unveils details of the molecular network: the pentyl chains point towards the center of the pores following a star-like shape and appear as fuzzy long protrusions due to their mobility at RT.[16] The pyridyl endgroups are imaged as small bright protrusions and point to a common three-fold node, which can also be seen as the vertex formed between three adjacent pores. Once again, the Ni-atom in the porphyrin core did not contribute to the STM contrast. The common three-fold node formed between the pyridyl endgroups could not be possible without an additional linker between them due to electrostatic repulsion between the electronegative N-atoms. Therefore, as illustrated in the tentative structural model (Figure 3e), the three-fold node is formed by metal-ligand interactions between one Co-atom

(orange circles) bonded to the N-atoms (blue circles) from three different pyridyl endgroups, resulting in a 1.5:1 molecule-to-metal ratio.[16] It is well known that 3d transition metals located at the coordination nodes on metal substrates often remain invisible under STM.[32–34] Nevertheless, our study supports the preference that Co-atoms have towards (in-plane) three-fold coordination on noble metal surfaces,[6,12,16,19,34–36] despite the fact that such coordination motifs have been rarely reported for pyridyl-substituted porphyrins.[16] It is worth to mention that the three-fold Co-coordinated node prevailed independently of: (i) the Ni-atom in the porphyrin core, since our results (Figure 3) are structurally comparable to our findings shown in our previous report of the free-base version (DPPyP) of Ni-DPPyP on Ag(111)[16] and (ii) the length of the alkyl endgroup, as the deposition of another analogue of Ni-DPPyP containing hexyl instead of pentyl chains gave rise to a structurally equivalent porous network after coordinating to Co-atoms on Au(111) (Supporting Information Figure S2).

Combining our STM and LEED data (Figure 3) we constructed a rhombic unit cell (black rhombus in Figure 3a and d) with dimensions $a = b = 32 \pm 0.2$ Å, and an internal angle of $\alpha = 60° \pm 2°$. This network has a molecular density of 0.34 Ni-DPPyP molecules per nm^2. In addition, a rotation of 15° between the unit cell axis and the principal Au directions was observed. The porous network is incommensurate with the underlying Au substrate, i.e., the absence of integer matrix elements in the superstructure matrix of the simulated LEED pattern (Figure 3d) supports this affirmation. Furthermore, the two rotational domains of the network are shown in gray and green in the simulated LEED pattern (Figure 3d).

In light of studying the formation of metal-ligand interactions in MOCNs on noble metal surfaces, the shift in the binding energies (BE) of a core level spectrum serve as a measure of the chemical environment of a particular atom prior to and after metal coordination.[8,33,37–40] Therefore, in addition to our STM and LEED data, we measured XP spectra for the C 1s, N 1s and Ni $2p_{3/2}$ core levels to check both the chemical composition and possible changes of the electronic structure of Ni-DPPyP on Au(111) before and after coordination with Co-atoms. Ni-DPPyP contains a total of six N-atoms and forty C-atoms distributed in two and five chemically different environments, respectively. Each group of chemically different atoms is properly labelled and color coded in the ball and stick model shown in Figure 4g. The two different chemical states of the N-atoms are given by: N1 (iminic N-atom coordinating to the central Ni-atom) and N2 (located in the pyridyl endgroup). On the other hand, the C-atoms are grouped as follows: four types of sp^2-hybridized C-atoms can be found as C1 (bonded to only C-atoms), C3 (located inside the pyrrole and pyridyl moieties bonded to C- and H-atoms), C4 (bonded to N1), C5 (bonded to N2); and one type of sp^3-hybdrized C-atoms labelled as C2 (placed along the pentyl chains and connected to C- and H-atoms).

The C 1s core level spectrum of the close-packed network (Figure 4a) was fitted with five components. For fitting the C 1s spectra, the FWHM of the components was allowed to vary between 0.5 eV and 0.7 eV, whereas the area ratios were left

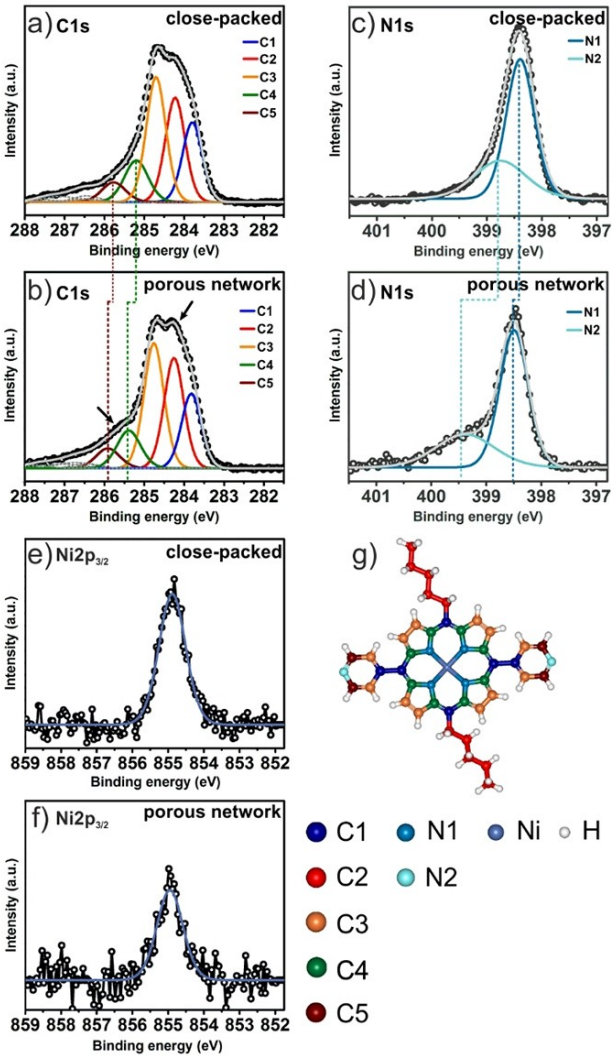

Figure 4. (a), (c), (e) C 1s, N 1s and Ni $2p_{3/2}$ core level spectra of Ni-DPPyP on Au(111) for the close-packed structure. (b), (d), (f) C 1s, N 1s and Ni $2p_{3/2}$ core level spectra of Ni-DPPyP on Au(111) for the cobalt-coordinated porous network. The black arrows in (b) point to the observable differences in the C 1s envelope of the porous network structure when compared to the C 1s envelope of the close-packed network. Due to the metal coordination, a peak shift towards higher binding energies of the C4, C5, N1 and N2 components was observed and is emphasized by the vertical dotted lines. (g) Ball and stick molecular model of Ni-DPPyP where the chemically different carbon and nitrogen species are color coded. The C 1s components (C1–C5) are correlated with the carbon components in (a) and (b). For peak positions see Table S1 and Table S2 in the Supporting Information. The C 1s and N 1s spectra were acquired with a photon energy $h\upsilon = 500$ eV, while the Ni $2p_{3/2}$ spectra were acquired with a photon energy $h\upsilon = 1.02$ keV.

free. The assignment of the components was done with respect to the stoichiometry of the molecule: C1:C2:C3:C4:C5 = 6:10:12:8:4. The BE for the components of the C 1s core level spectra can be found in Table S1 in the Supporting Information. The main component (orange peak) located at 284.71 eV was attributed to C3 and is in line with the BE values reported for aromatic carbons.[41–46] The second largest contribution (red peak) located at 284.23 eV belongs to C2 and agrees with the peak positions reported for sp^3-hybdrized C-atoms in alkyl

chains.[47–49] The green peak (285.20 eV) corresponds to C4 which is bonded to the N-atoms from the porphyrin core. C4 appears at a higher BE as compared with C1, C2, and C3 due to its near proximity to the N-atom (N1), which possesses an increased electronegativity as compared with the C-atom. Thus, the N1-atom pulls the carbon valence electrons strongly away from the C4-atoms lowering its electron density, which leads to an effective increase of its nuclear charge and it therefore increases the BE observed in the C 1s spectrum.[24,44,45] The contribution at the lowest BE (283.80 eV) was attributed to C1 and resembles the C–C bonds along the porphyrin backbone.[50] Finally, the smallest contribution (brown peak) was given to C5 and is located at the highest BE (285.77 eV) because it is bonded to the pyridylic N-atoms (N2) involved in H-bonding.[24] Thus, similarly to the case of C4, the N-atoms (N2) bonded to H-atoms pull electron density away from C5.

The N 1s core level spectrum of the close-packed network (Figure 4c) was fitted with two components. For fitting the N 1s spectra, the area ratios were fixed to 4:2 and the FWHM was left free. The energy position for each component of the N 1s spectrum can be found in Table S2 in the Supporting Information. The peak located at 398.75 eV was attributed to N2, since the pyridylic N-atom (N2) is bonded to a H-atom and consequently, appears at a slightly higher BE than the N-atoms (N1) contained in the porphyrin core which are bonded to a Ni-atom. This peak position is consistent with the one obtained for pyridylic N-atoms in tetrapyridyl-substituted porphyrins.[22] In addition, in previous reports for free-base porphyrins, the N-atoms bonded to H-atoms in the porphyrin core have been assigned to higher BE than their iminic counterparts (N-atoms in the porphyrin core with an electron lone pair) and can be compared to the chemical environment that N2 has while being bonded to a neighboring H-atom.[23,51–53] Therefore, the peak at lower BE (398.39 eV) was assigned to N1 as compared with the values reported for iminic N-atoms in Ni-substituted porphyrins[53–55] and in various metal-substituted porphyrins on noble metal surfaces.[22,23,52,56]

The deposition of Co-atoms and subsequent annealing led to the formation of a porous 2D network as previously mentioned. The C 1s core level spectrum of the porous 2D network (Figure 3) is shown in Figure 4b. Similar to the C 1s spectrum of the close-packed network, the intensity ratio between the components is in line with the stoichiometric ratio of C-atoms (also see Supporting Information Table S2). However, by comparing the C 1s envelopes of both networks (Figure 4a and b), a modification in the shape of the C 1s envelope of the porous network (Figure 4b) can be seen as highlighted by the black arrows. In addition, a chemical shift (highlighted by the vertical green line) of 0.19 eV and a spectral shift of 0.14 eV (highlighted by the vertical brown dotted line) towards higher BE was observed for the C4 (green peak) and C5 (brown peak) components, respectively. Similarly, the N 1s envelope (Figure 4d) of the porous 2D network presented new features that were given by a marked shift (highlighted by the vertical dark blue and turquoise dotted lines) of 0.10 eV and 0.67 eV towards higher BE of the N1 (dark blue peak) and N2 (turquoise peak) components, respectively. The most pronounced chemical shift was observed for N2 at 399.49 eV and can be explained by the Co-directed structural transformation going from H-bonding (Figure 1) to metal-ligand coordination (Figure 3) where the nuclear charge of N2 increases after donating charge to the Co-atoms.[22,33,57] Consequently, N2 withdraws charge from C5 which leads to a spectral shift (brown peak) of 0.14 eV. Similar chemical shifts have been reported for the pyridylic N 1s signal of tetrapyridyl-porphyrins coordinating to Cu-atoms and linear bis-pyridyl molecules coordinating to Fe-atoms on Au(111).[22,57]

On the other hand, the smaller shifts of C4 (0.19 eV) and N1 (0.10 eV) might be an indication of a possible conformational change of the porphyrin core due to the metal coordination observed between the pyridyl endgroups and Co-atoms. We hypothesize that upon MOCN formation the central Ni-atom of the porphyrin might be slightly lifted (away) from the Au surface as compared with the close-packed structure. Thus, a possible weakened interaction between the Ni-atoms and the Au surface results in an increased interaction between the Ni-atoms with the N-atoms of the porphyrin core, which translates into a shift towards higher BE for N1 and C4. Similar conformational adaptations of the porphyrin core that modify its distance to the underlying surface by the dihedral rotation of the aromatic endgroups have been previously reported.[46] Thus, we consider the possibility that the pyridyl endgroups of the Ni-DPPyP derivatives are tilted with a large dihedral angle with respect to the Au surface, which elevates the porphyrin core.[46] In addition, the Ni $2p_{3/2}$ core level spectra taken before (Figure 4e) and after (Figure 4f) metal-coordination can be taken as support for our assumption. Even if the chemical shift (0.07 eV) is small, it can be an indication that the Ni-atom could have increased its charge after being separated from the Au surface. Additionally, the BE of the Ni $2p_{3/2}$ core level is in agreement with the reported values for a nickel-substituted tetraphenyl porphyrin (NiTPP) on Au(111) and a nickel-substituted tetrabromophenyl porphyrin (NiTBrPP) on Cu-(111).[54,58]

As previously mentioned, the results shown in the present study are in good agreement with the results from our earlier study of the free-base version of Ni-DPPyP adsorbed on Ag(111).[16] The main similarities are the overall structures of the 2D networks and bonding motifs found within each structure, i.e., H-bonding stabilizing the organic phases, whereas a three-fold Co-coordination motif is present in the porous MOCNs. However, there are a few differences that we would like to address in the following in terms of: (i) influence of the underlying substrate: Au(111) vs. Ag(111) and (ii) the role of the Ni-atom in the core of Ni-DPPyP. In terms of (i) the underlying substrate, the lattice constants of Au and Ag are very similar and their reactivity can be considered relatively low with Au being less reactive. Therefore, the formation of structurally equivalent phases on both substrates can be expected. Furthermore, in our previous study the formation of the MOCN on Ag(111) took place at room temperature, whereas on Au(111) the MOCN was formed upon post-deposition annealing at 423 K. In contrast, the porous network on Ag(111) transformed back into the close-packed network upon annealing at

450 K. This suggests, since the annealing temperatures are similar, that the stability of the MOCN on Au(111) could be higher. The difference in stability between the porous MOCNs may be influenced by (ii) the interaction of the porphyrin core with the substrate. On Ag(111), a metal-free porphyrin was used and its interaction with the substrate can expected to be different compared to Ni-DPPyP adsorbed on Au(111).[41] A metalation of its core upon annealing the MOCN at 450 K is a reasonable assumption. This means the coordinating Co-atoms of the MOCN could then have metalized the porphyrin core and the MOCN transformed back into a close-packed network. Since on Au(111) a Ni-substituted porphyrin was used no metalation reaction can occur.

Conclusion

We have presented a complementary study of the influence of Co-deposition on the self-assembly process of a Ni-substituted porphyrin derivative (Ni-DPPyP) on Au(111) by means of STM, LEED and XPS. As revealed by STM, the deposition of Ni-DPPyP for coverages <1 monolayer on Au(111) formed a well-ordered close-packed network stabilized by H-bonding between the N-atoms of the pyridyl endgroups and the H-atoms from neighboring pyrrole moieties. The long-range order of this 2D network was corroborated by LEED measurements. In addition, the chemical state of the C- and N-atoms – prior to Co-deposition – was investigated with XPS, which agreed with the previously reported BE for the C 1s and N 1s core levels in porphyrin-based 2D networks stabilized by H-bonding on metal surfaces.

The deposition of Co-atoms onto the close-packed network led to a structural transformation, i.e., the formation of a Co-coordinated hexagonal porous network. The long-range order of the network was revealed by LEED measurements. The presence of metal-ligand interactions was confirmed by XPS with a marked chemical shift (0.67 eV) towards higher BE of the pyridylic N 1s XPS signal of the hexagonal porous network. Furthermore, the small spectral shifts in the C 1s XPS signal also provided information on the possible conformational change of the porphyrin core after the deposition of Co-atoms. Therefore, while STM measurements allow studying the structure of MOCNs and give insight to the lateral interactions within these structures, XPS can provide complementary information of the chemical environment of the atomic species within the MOCN in order to confirm the nature of the lateral interactions stabilizing the network and may even suggest possible conformational changes within the molecules adsorbed on the surface.

Experimental Section

The STM and LEED experiments were carried out in two ultra-high vacuum (UHV) systems (with a base pressure in the 5×10^{-10} mbar regime) equipped with different chambers for sample preparation and characterization. Each UHV system hosts a STM (Scienta Omicron GmbH) that was either operated at (i) room temperature or (ii) 77 K. The Au(111) single crystal was cleaned by repeated cycles of Ar^+ sputtering and annealing at 750 K. The porphyrin derivatives (Ni-DPPyP)[16] were sublimed at 460 K onto the Au(111) surface using a home-built evaporator. Cobalt atoms were deposited onto the Ni-DPPyP layer from a cobalt rod using an e-beam evaporator (Oxford Applied Research). During both depositions (molecule and metal) the Au(111) substrate was held at RT. The molecule and metal deposition rates were monitored with a quartz crystal microbalance. The STM measurements were performed in the constant current mode with a tip which was mechanically cut from a Pt/Ir (90/10 chemical composition) wire. All bias voltages are given with respect to a grounded tip. The STM images were processed with WSxM software.[24] Additionally, the LEED patterns were acquired using a commercial LEED setup (Specs ErLEED 150) and simulated with LEEDPat4.2 software.[25] Furthermore, the XPS measurements were performed at the I09 beam line at the Diamond Light Source (Oxfordshire, UK). Sample preparation and measurements were performed in situ under UHV conditions. As confirmed by the LEED measurements at the I09 beam line, the structural arrangement of both networks (close-packed and porous) was successfully reproduced. The analysis chamber contained a VG Scienta EW4000 HAXPES hemispherical photoelectron analyzer. The C 1s and N 1s core level spectra were acquired using a photon energy of 500 eV, while the Ni $2p_{3/2}$ spectra were acquired with a photon energy of 1.02 keV. The BE scale of the XPS data was calibrated to the Au $4f_{7/2}$ peak at 84.0 eV. For all the spectra a linear background was subtracted. The XPS spectra were fitted with Voigt profiles (convolution of a Gaussian and a Lorentzian).

Acknowledgements

This work was supported by the Netherlands Organization for Scientific Research (NWO) (Vici grant 680-47-633 and Veni grant 722.012.010), by the Foundation for Fundamental Research on Matter (FOM), part of NWO, and the Zernike Institute for Advanced Materials of the University of Groningen. University of Strasbourg, CNRS, Institut Universitaire de France (IUF), and the International Center for Frontier Research in Chemistry (icFRC) and the Ministry of Education and Research (scholarship to N.M.) are acknowledged for financial support to the Strasbourg group.

Conflict of Interest

The authors declare no conflict of interest.

Keywords: metal-organic coordination networks · molecular self-assemblies · scanning tunneling microscopy · X-ray photoelectron spectroscopy

[1] D. P. Goronzy, M. Ebrahimi, F. Rosei, Arrmael, Y. Fang, S. De Feyter, S. L. Tait, C. Wang, P. H. Beton, A. T. S. Wee, P. S. Weiss, D. F. Perepichka, *ACS Nano* **2018**, *12*, 7445–7481.
[2] H. Furukawa, K. E. Cordova, M. O'Keeffe, O. M. Yaghi, *Science* **2013**, *341*, 1230444.
[3] A. Bétard, R. A. Fischer, *Chem. Rev.* **2012**, *112*, 1055–1083.
[4] J. V. Barth, *Surf. Sci.* **2009**, *603*, 1533–1541.
[5] R. Gutzler, S. Stepanow, D. Grumelli, M. Lingenfelder, K. Kern, *Acc. Chem. Res.* **2015**, *48*, 2132–2139.
[6] L. Dong, Z. A. Gao, N. Lin, *Prog. Surf. Sci.* **2016**, *91*, 101–135.

[7] B. D. Baker Cortés, M. Stöhr, in *Encycl. Interfacial Chem.* (Ed.: K. Wandelt), Elsevier, **2018**, *4*, pp 153–165.
[8] F. Klappenberger, *Prog. Surf. Sci.* **2014**, *89*, 1–55.
[9] B. D. Baker Cortés, N. Schmidt, M. Enache, M. Stöhr, *J. Phys. Chem. C* **2019**, *123*, 19681–19687.
[10] W. Auwärter, D. Écija, F. Klappenberger, J. V. Barth, *Nat. Chem.* **2015**, *7*, 105–120.
[11] J. M. Gottfried, *Surf. Sci. Rep.* **2015**, *70*, 259–379.
[12] T. A. Pham, F. Song, M. N. Alberti, M.-T. Nguyen, N. Trapp, C. Thilgen, F. Diederich, M. Stöhr, *Chem. Commun.* **2015**, *51*, 14473–14476.
[13] L.-A. Fendt, M. Stöhr, N. Wintjes, M. Enache, T. A. Jung, F. Diederich, *Chem. Eur. J.* **2009**, *15*, 11139–11150.
[14] Z. Shi, N. Lin, *J. Am. Chem. Soc.* **2009**, *131*, 5376–5377.
[15] X. F. Mao, T. Lin, J. Adisoejoso, Z. Shi, X. S. Shang, P. N. Liu, N. Lin, *Phys. Chem. Chem. Phys.* **2013**, *15*, 12447.
[16] F. Studener, K. Müller, N. Marets, V. Bulach, M. W. Hosseini, M. Stöhr, *J. Chem. Phys.* **2015**, *142*, 101926–1/101926–6.
[17] S. Nowakowska, F. Mazzola, M. N. Alberti, F. Song, T. Voigt, J. Nowakowski, A. Wäckerlin, C. Wäckerlin, J. Wiss, W. B. Schweizer, M. Broszio, C. Polley, M. Leandersson, S. Fatayer, T. Ivas, M. Baljozovic, S. F. Mousavi, A. Ahsan, T. Nijs, O. Popova, J. Zhang, M. Muntwiler, C. Thilgen, M. Stöhr, I. Pasti, N. Skorodumova, F. Diederich, J. Wells, T. A. Jung, *ACS Nano* **2018**, 12, 768–778.
[18] D. Kühne, F. Klappenberger, R. Decker, U. Schlickum, H. Brune, S. Klyatskaya, M. Ruben, J. V. Barth, *J. Am. Chem. Soc.* **2009**, *131*, 3881–1883.
[19] U. Schlickum, R. Decker, F. Klappenberger, G. Zoppellaro, S. Klyatskaya, M. Ruben, I. Silanes, A. Arnau, K. Kern, H. Brune, J. V. Barth, *Nano Lett.* **2007**, *7*, 3813–3817.
[20] T. R. Umbach, M. Bernien, C. F. Hermanns, A. Krüger, V. Sessi, I. Fernandez-Torrente, P. Stoll, J. I. Pascual, K. J. Franke, W. Kuch, *Phys. Rev. Lett.* **2012**, *109*, 267207.
[21] W. Jiang, X. Ni, F. Liu, *Acc. Chem. Res.* **2021**, *54*, 416–426.
[22] Y. Li, J. Xiao, T. E. Shubina, M. Chen, Z. Shi, M. Schmid, H.-P. Steinrück, J. M. Gottfried, N. Lin, *J. Am. Chem. Soc.* **2012**, *134*, 6401–6408.
[23] J. M. Gottfried, K. Flechtner, A. Kretschmann, T. Lukasczyk, H.-P. Steinrück, *J. Am. Chem. Soc.* **2006**, *128*, 5644–5645.
[24] M. R. Cohen, *Surf. Sci.* **1991**, *245*, 1–11.
[25] I. Horcas, R. Fernández, J. M. Gómez-Rodríguez, J. Colchero, J. Gómez-Herrero, A. M. Baro, *Rev. Sci. Instrum.* **2007**, *78*, 013705.
[26] K. Hermann, M. A. van Hove. LEEDpat4 (LEED pattern analyzer). http://www.fhi-berlin.mpg.de/KHsoftware/LEEDpat/index.html (accessed January 19, 2021).
[27] W. Auwärter, A. Weber-Bargioni, A. Riemann, A. Schiffrin, *J. Chem. Phys.* **2006**, *124*, 194708.
[28] Y. Wang, K. Zhou, Z. Shi, Y.-Q. Ma, *Phys. Chem. Chem. Phys.* **2016**, *18*, 14273.
[29] D. Rolf, C. Lotze, C. Czekelius, B. W. Heinrich, K. J. Franke, *J. Phys. Chem. Lett.* **2018**, *9*, 6563–6567.
[30] F. Buchner, I. Kellner, W. Hieringer, A. Görling, H.-P. Steinrück, H. Marbach, *Phys. Chem. Chem. Phys.* **2010**, *12*, 13082–13090.
[31] W. Auwärter, A. Weber-Bargioni, S. Brink, A. Riemann, A. Schiffrin, M. Ruben, J. V. Barth, *ChemPhysChem* **2007**, *8*, 250-.254.
[32] J. Björk, M. Matena, M. S. Dyer, M. Enache, J. Lobo-Checa, L. H. Gade, T. A. Jung, M. Stöhr, M. Persson, *Phys. Chem. Chem. Phys.* **2010**, *12*, 8815–8821.
[33] M. Matena, J. Björk, M. Wahl, T.-L. Lee, J. Zegenhagen, L. H. Gade, T. A. Jung, M. Persson, M. Stöhr, *Phys. Rev. B* **2014**, *90*, 125408–1/125408–8.
[34] N. Henningsen, R. Rurali, C. Lumbach, R. Drost, J. I. Pascual, K. J. Franke, *J. Phys. Chem. Lett.* **2011**, *2*, 55–61.
[35] M. W. Hosseini, *Acc. Chem. Res.* **2005**, *38*, 313–323.
[36] S. Stepanow, N. Lin, D. Payer, U. Schlickum, F. Klappenberger, G. Zoppellaro, M. Ruben, H. Brune, J. V. Barth, K. Kern, *Angew. Chem. Int. Ed.* **2007**, *46*, 710–713; S. Stepanow, N. Lin, D. Payer, U. Schlickum, F. Klappenberger, G. Zoppellaro, M. Ruben, H. Brune, J. V. Barth, K. Kern, *Angew. Chem.* **2007**, *119*, 724–727.
[37] U. Gelius, *Phys. Scr.* **1974**, *9*, 133–147.
[38] C. D. Tempas, D. Skomski, B. J. Cook, D. Le, K. A. Smith, T. S. Rahman, K. G. Caulton, S. L. Tait, *Chem. Eur. J.* **2018**, *24*, 15852–15858.
[39] Q. Shen, E. J. Larkin, C. Delaney, Y. Cheng, C. Miao, X. Zhou, L. Liu, W. Huang, H. Gao, S. M. Draper, H. Fuchs, *J. Phys. Chem. C* **2018**, *122*, 8954–8959.
[40] K. Müller, J. C. Moreno-López, S. Gottardi, U. Meinhardt, H. Yildirim, A. Kara, M. Kivala, M. Stöhr, *Chem. Eur. J.* **2016**, *22*, 581–589.
[41] T. Lukasczyk, K. Flechtner, L. R. Merte, N. Jux, F. Maier, J. M. Gottfried, H.-P. Steinrück, *J. Phys. Chem. C* **2007**, *111*, 3090–3098.
[42] C. Ronning, H. Feldermann, R. Merk, H. Hofsass, *Phys. Rev. B* **1998**, *4*, 2207–2215.
[43] A. M. Ektessabi, S. Hakamata, *Thin Solid Films* **2000**, *377–378*, 621–625.
[44] K. Shen, B. Narsu, G. Ji, H. Sun, J. Hu, Z. Liang, X. Gao, H. Li, Z. Li, B. Song, Z. Jiang, H. Huang, J. W. Wells, F. Song, *RSC Adv.* **2017**, *7*, 13827.
[45] H. Peisert, M. Knupfer, J. Fink, *Surf. Sci.* **2002**, *515*, 491–498.
[46] J. Xiao, S. Ditze, M. Chen, F. Buchner, M. Stark, M. Drost, H.-P. Steinrück, J. M. Gottfried, H. Marbach, *J. Phys. Chem. C* **2012**, *116*, 12275–12282.
[47] F. Cecchet, M. Pilling, L. Hevesi, S. Schergna, J. K. Y. Wong, G. J. Clarkson, D. A. Leigh, P. Rudolf, *J. Phys. Chem. B* **2003**, *107*, 10863–10872.
[48] D. Wilson, M. A. Langell, *Appl. Surf. Sci.* **2014**, *303*, 6–13.
[49] N. Graf, E. Yegen, T. Gross, A. Lippitz, W. Weigel, S. Krakert, A. Terfort, W. E. S. Unger, *Surf. Sci.* **2009**, *603*, 2849–2860.
[50] C. Bürker, A. Franco-Cañellas, K. Broch, T.-L. Lee, A. Gerlach, F. Schreiber, *J. Phys. Chem. C* **2014**, *118*, 13659–13666.
[51] F. Buchner, J. Xiao, E. Zillner, M. Chen, M. Röckert, S. Ditze, M. Stark, H.-P. Steinrück, J. M. Gottfried, H. Marbach, *J. Phys. Chem. C* **2011**, *115*, 24172–24177.
[52] A. Kretschmann, M.-M. Walz, K. Flechtner, H.-P. Steinrück, J. M. Gottfried, *Chem. Commun.* **2007**, 568–570.
[53] T. E. Shubina, H. Marbach, K. Flechtner, A. Kretschmann, N. Jux, F. Buchner, H.-P. Steinrück, T. Clark, J. M. Gottfried, *J. Am. Chem. Soc.* **2007**, *129*, 9476–9483.
[54] M. Chen, X. Feng, L. Zhang, H. Ju, Q. Xu, J. Zhu, J. M. Gottfried, K. Ibrahim, H. Qian, J. Wang, *J. Phys. Chem. C* **2010**, *114*, 9908–9916.
[55] C. Wang, Q. Fan, Y. Han, J. I. Martínez, J. A. Martín-Gago, W. Wang, H. Ju, J. M. Gottfried, J. Zhu, *Nanoscale* **2016**, *8*, 1123–1132.
[56] G. Di Santo, C. Castellarin-Cudia, M. Fanetti, B. Taleatu, P. Borghetti, L. Sangaletti, L. Floreano, E. Magnano, F. Bondino, A. Goldoni, *J. Phys. Chem. C* **2011**, *115*, 4155–4162.
[57] D. Hötger, P. Carro, R. Gutzler, B. Wurster, R. Chandrasekar, S. Klyatskaya, M. Ruben, R. C. Salvarezza, K. Kern, D. Grumelli, *Phys. Chem. Chem. Phys.* **2018**, *20*, 15960–15969.
[58] C. M. Doyle, J. P. Cunniffe, S. A. Krasnikov, A. B. Preobrajenski, Z. Li, N. N. Sergeeva, M. O. Senge, A. A. Cafolla, *Chem. Commun.* **2014**, *50*, 3447.

Manuscript received: April 6, 2021
Accepted manuscript online: June 21, 2021
Version of record online: July 22, 2021

